A structure-function study of ZraP and ZraS provides new insights into the two-component system Zra

Raleb Taher, Eve de Rosny

A structure-function study of ZraP and ZraS provides new insights into the two-component system Zra.

Raleb Taher[1,2], Eve de Rosny[1,*]

[1]Univ. Grenoble Alpes, CEA, CNRS, IBS, Metalloproteins Unit, F-38000 Grenoble, France
[2]Current address: University of California, Irvine, Medical Science Building B, CA 92697

* Corresponding author

Abstract:

Background
Zra belongs to the envelope stress response (ESR) two-component systems (TCS). It is atypical because of its third periplasmic repressor partner (ZraP), in addition to its histidine kinase sensor protein (ZraS) and its response regulator (ZraR) components. Furthermore, although it is activated by Zn^{2+}, it is not involved in zinc homeostasis or protection against zinc toxicity. Here, we mainly focus on ZraS but also provide information on ZraP.
Methods
The purified periplasmic domain of ZraS and ZraP were characterized using biophysical and biochemical technics: multi-angle laser light scattering (MALLS), circular dichroism (CD), differential scanning fluorescence (DSF), inductively coupled plasma atomic emission spectroscopy (ICP-AES), cross-linking and small-angle X-ray scattering (SAXS). *In-vivo* experiments were carried out to determine the redox state of the cysteine residue in ZraP and the consequences for the cell of an over-activation of the Zra system.
Results
We show that ZraS binds one Zn^{2+} molecule with high affinity resulting in conformational changes of the periplasmic domain, consistent with a triggering function of the metal ion. We also demonstrate that, in the periplasm, the only cysteine residue of ZraP is at least partially reduced. Using SAXS, we conclude that the previously determined X-ray structure is different from the structure in solution.
Conclusion
Our results allow us to propose a general mechanism for the Zra system activation and to compare it to the homologous Cpx system.
General significance
We bring new input on the so far poorly described Zra system and notably on ZraS.

Keywords: Zra system; ZraS; ZraP; two-component systems; envelope stress response; zinc binding proteins

1. Introduction

Two-component systems (TCS) are widely used by gram-negative bacteria to respond to changes in the environment. They allow communication between the periplasm and the cytoplasm via transmembrane signal transduction pathways. Classical TCS are composed of two interacting partners, a transmembrane histidine kinase sensor protein (HK) and a cytoplasmic response regulator (RR). The external signals are sensed by the periplasmic domain of the HKs resulting in the autophosphorylation of a cytoplasmic histidine. The phosphate group is then transferred to a specific aspartic acid of the cognate RR protein leading to its activation. Based on the genomic sequence, 29 genes coding HK are predicted by the P2CS database in the non-pathogenic K12 *E. coli* [1]. Twenty-four of these HKs were characterized and studied in association with their cognate RR. TCS are generally involved in several cellular responses to environmental conditions, such as metabolism adaptation, metal homeostasis, motility, quorum sensing and envelope stress response. Due to their ability to detect environmental changes during infection many TCSs present in pathogenic strains are involved in virulence and antibiotic resistance. In the archetypal mechanism, the signaling effector is a small molecule that binds

to the ligand binding pocket of the periplasmic HK domain and induces local conformational modifications that are transmitted to the intracellular domain via a piston-type movement of one of the transmembrane helices [2]. For many TCS, the activating mechanism is more complex than the simple binding of the effector molecule because it requires additional accessory sensing proteins. The Cpx and Zra TCS are atypical in the sense that their pathways involve a repressor accessory protein. Cpx senses the envelope stress generated by numerous environmental factors. It is proposed to respond to misfolded periplasmic proteins [3]. Several lines of evidence indicate that the periplasmic CpxP protein inhibits CpxA kinase activity by direct interaction; its release would then be promoted by either binding to unfolded proteins or by disruption of the polar interactions at the interface of CpxA and CpxP [4–6]. Like in the case of CpxP and CpxA, ZraP was shown to be a repressor of ZraS activity [7,8]. However, while CpxA appears to be directly active upon CpxP dissociation, ZraS activation requires the presence of activating metal ions. Experiments with *zraP*-mutant *E. coli* strain (*ΔzraP*) showed that the expression of genes regulated by ZraR is activated by Zn^{2+}, Pb^{2+} and, to a much lesser extent, by other metal ions such as Cd^{2+}, Ni^{2+} and Cu^{2+}. This activation was about two-fold higher with zinc compared to lead, suggesting that zinc is the best inducer of ZraS activation [8]. Remarkably, although for all described TCS the triggering signal is directly related to the cellular response, there is no evidence of a ZraS-ZraP involvement in protection against zinc toxicity or zinc homeostasis [7–9]. Another puzzling aspect is that zinc acts at two levels: it activates the Zra system and binds the repressor protein ZraP with high affinity [8]. These observations make the physiological role of the metal ion unclear. Until very recently nothing was known about the Zra regulon except that it up-regulates the expression of its own components [10]. *ZraS* and *zraR* are localized in the same locus as *zraP,* but they are controlled by a different and much weaker promoter, resulting in higher ZraP production compared to ZraS and ZraR [8]. A recent publication highlighted the Zra regulon and confirmed that it is involved in envelope stress response [11]. This had been initially postulated from its involvement in polymixin protection and from the ZraP *in vitro* chaperon activity [7,8].
Most of the publications about the Zra system have provided information on ZraP from *Escherichia coli* and *Salmonella enterica.* The two *ZraP* proteins share 69% identity and have the same functions. Notably, they are repressors of the Zra system and have *in vitro* zinc-dependent chaperon activity [7,8]. However, very little has been reported on ZraS, except that it responds to zinc and lead ions [8]. Here, we focus on ZraS but also provide new data on the ZraP redox state in the periplasm and on its SAXS solution structure. We demonstrate that the periplasmic domain of ZraS binds one Zn^{2+} molecule with high affinity and show that this binding induces conformational changes, consistent with the metal ion playing a triggering function. In addition, we show that, *in vivo*, the only ZraP cysteine is reduced, even though it was previously described, in the purified protein, as forming a disulfide bond between two subunits [8]. The analysis of our results along with the previously published ones allow us to propose a general mechanism for Zra activation.

2. Materials and methods

2.1. ZraSp expression and purification

The coding sequence of ZraS periplamic domain was amplified by PCR from *E. coli* genomic DNA and cloned into the pASK-IBA7+ plasmid via the BsaI restriction sites, leading to the following open reading frame:
MASWSHPQFEKIEGRDYGRASEADRQALLEKGNVLIRALESGSRVGMGMRMHHVQQQALL
EEMAGQPGVLWFAVTDAQGIIILHSDPDKVGRALYSPDEMQKLKPEENSRWRLLGKTETTPA
LEVYRLFQPMSAPWRHGMHNMPRCNGKAVPQVDAQQAIFIAVDASDLVATQSGEKRNT.
MASWSHPQFEKIEGR corresponds to the strep tag and linker sequences that are provided by the pASK-IBA7+, and the rest of the sequence to residues 37-202 of ZraS.
Protein expression was performed in *E. coli* strain BL21(DE3). Cells were grown under agitation with 100 µg/mL of ampicillin at 37 °C in LB media to an OD_{600nm} of 0.8 before addition of 200 ng/mL of anhydrotetracycline. Then, the temperature was adjusted to 18°C for overnight expression of ZraSp. After centrifugation, the cell pellet was resuspended in 50 mM HEPES pH 7.5, 100 mM NaCl, complemented with a tablet of EDTA-free protease Inhibitor cocktail (Roche) and lysed by sonication.

The crude extract was recovered in the supernatant after centrifugation at 15,000 rpm for 30 min at 4°C.
The crude extract was loaded onto a 10 mL StrepTactin-affinity column equilibrated with buffer A1 (50 mM HEPES pH 7.5, 100 mM NaCl) and washed with 30 mL of buffer A1. Elution of strep-tagged ZraSp was performed by addition of 20 mL of buffer B1 (50 mM, HEPES pH 7.5, 100 mM NaCl, 2.5 mM desthiobiotin). The fractions were analyzed by SDS-PAGE, and those containing ZraSp were pooled and concentrated by ultrafiltration. Then, the protein solution was injected onto a HiLoad 16/60 Superdex 75 gel filtration column (GE Healthcare life Science) equilibrated with buffer A1. Fractions containing pure protein were stored at -80°C.

2.2. Circular dichroism

CD measurements were performed with 3.54 µM of ZraSp in 20 mM potassium-phosphate pH 7.5 with a JASCO J-1500 circular dichroism spectrometer (JASCO Analytical Instruments) and a cell path length of 0.1 cm. The spectra were recorded from 190 to 240 nm with a data pitch of 1 nm and a scan speed of 100 nm/min. Either 5 or 10 µL of a 82 µM $ZnSO_4$ solution diluted in 20 mM phosphate buffer were successively added to the cuvette, to reach 0.45, 0.89, 1.34 and 1.78 ZraSp-Zn^{2+} molar ratios. For each condition, 10 spectra were accumulated and ellipticity values were adjusted to compensate for dilutions. Secondary structures were analyzed with the Dichroweb tool using the CDSSTR method, set7 optimized for 190-240 nm [12,13].

2.3. Thermal unfolding

Melting temperatures were measured using a Prometheus NT.48 (Nanotemper). A solution of 50 µM (1 mg/mL) ZraSp diluted in 100 mM NaCl, 50 mM HEPES pH 7.5 was first passed through a 0.20 µm filter to remove aggregates before transferring it to microtubes and addition of 0 to 62.5 µM $ZnSO_4$ concentrations. Samples were kept on ice before transfer into capillaries. Heating was performed at a rate of 2°C.min^{-1} from 20 to 95°C. Fluorescence emission was measured at 330 and 350 nm. It was verified that the fluorescence of zinc, in the absence of protein, was stable in the buffer. Data were fitted to a two-state model, according to the equation below [14] using KaleidaGraph 3.6 (synergy software).

$$F = \frac{(F_i + a_i \cdot T) + (F_f + a_f \cdot T) \cdot e^{\left(\left(\frac{\Delta H_m}{R}\right) \cdot \left(\frac{1}{T_m} - \frac{1}{T}\right)\right)}}{1 + e^{\left(\left(\frac{\Delta H_m}{R}\right) \cdot \left(\frac{1}{T_m} - \frac{1}{T}\right)\right)}}$$

F: F_{330nm}/F_{350nm}; F_i et F_f baseline intercept corresponding to initial (native protein) and final (denatured protein) conditions, a_i and a_f baseline slope; T: temperature; R: gas constant. The fitted parameters are melting temperature T_m, and enthalpy change ΔH_m. The experiment was performed in duplicate and gave similar results (not shown).

2.4. Size exclusion chromatography multi-angle laser light scattering (SEC-MALLS)

The quarternary structure of ZraSp was determined by size exclusion chromatography coupled to a multi-angle laser light scatter and refractometer. A volume of 20 µL of ZraSp at 4 mg/mL was loaded onto an analytical Superdex 75 10/300 GL equilibrated with 150 mM NaCl, 50 mM HEPES pH 7.5, at 4°C, connected to a miniDAWN TREOS Multi-Angle Light Scattering detector (Wyatt Instruments). The protein concentration was measured with the refractive index detector Optilab rEX, (Wyatt Instruments). Data analysis was performed using ASTRA, version 5.4.3.20 (Wyatt Instruments) and a refractive index increment (dn/dc) of 0.189 mL g^{-1}. Analytical size exclusion chromatography was performed at 4°C with a flow rate of 0.5 mL min^{-1}.

2.5. Cross-linking

A volume of 10 µL of an 80 µM ZraSp solution was incubated 35 min at room temperature in the presence of either 100 or 500 molar equivalents of formaldehyde, in 100 mM NaCl, 50 mM HEPES pH 7.5. The reaction was stopped by addition of denaturing Laemmli buffer before performing 15% SDS–PAGE. Samples were not heated before migration to avoid cross-link dissociations.

2.6. Zn^{2+} dosage by ICP-AES

Inductively coupled plasma atomic emission spectroscopy was performed with a Shimadzu ICP 9000 instrument. Standard solutions of zinc and ytterbium for ICP (Sigma-Aldrich) were used for quantification and internal standardization. Samples were prepared as follows: either 75 µL or 190 µL of 90 µM ZraSp were incubated in the presence of 4 molar $ZnSO_4$ equivalents plus either EDTA or EGTA at room temperature. As a negative control, 50 µL of ZraSp were incubated in the presence of 100 mM NaCl, 50 mM HEPES pH 7.5. Volumes were adapted to avoid protein precipitation, as detected in preliminary experiments. After 10 min incubation at room temperature, samples were dialyzed twice against 500 mL HEPES /NaCl buffer at 4°C for over 4 hours. They were then centrifuged 20 min at 15,000 rpm to eliminate precipitated proteins and stored at -20°C. Before the ICP-AES measurement, protein concentrations were determined by measuring their OD_{280nm} with a NanoDrop-2000 (Thermo Fisher Scientific Inc.) and an absorption coefficient of 26,470 $M^{-1}cm^{-1}$ calculated by ProtParam (ExPASy Server). The different samples were then treated with 65% HNO_3 to a final volume of 600 µL before a two-hour incubation at 70°C. Then, 5.4 mL of 10% HNO_3 were added before the measurement. The results provided by the spectrometer in µg/L of Zn^{2+} were converted into molar concentrations for Zn^{2+}/ZraSp molar ratio calculations.

2.7. Redox state of ZraP cysteine

The DNA sequence corresponding to *zraP* was cloned into the pBad18 plasmid between the SacI and SalI restriction sites. The *E. coli* W3110-*ΔzraR* strain was transformed with pBad-*zraP* and cells were grown in 30 mL LB in the presence of 20 µg/mL chloramphenicol and 0.1% arabinose, with or without 500 µM $ZnSO_4$, to an $OD_{600nm} \approx 0.8$. The *ΔzraR* mutant strain was chosen to prevent induction of the endogenous *zra* operon when zinc ions were added. In parallel, *E. coli* W3110 was grown in the presence of 500 µM $ZnSO_4$ to an $OD_{600nm} \approx 0.8$ for the expression of endogenous ZraP.
Two mL of this cell culture were centrifuged and the pellet was immediately resuspended with 100 µL of 1X denaturing Leammli buffer devoid of reducing agents and stored at -20°C. Then, 20 µL of the lysate were run on 15% SDS-PAGE. The protein was then transferred on a nitrocellulose membrane with the Trans-Blot Turbo Transfer System (Bio-Rad). Polyclonal anti-ZraP antibodies were used at a dilution of 1/3000 and horseradish peroxidase (HRP)-conjugated secondary antibody were detected by chemiluminescence with Clarity Western ECL Substrate and ChemiDoc imaging system (Bio-Rad)

2.8. Small-angle X-ray scattering (SAXS)

In order to get a homogeneous protein sample, a purified solution of ZraP [8] was injected onto a HiLoad 10/30 Superdex S200 gel filtration column (GE Healthcare) equilibrated with 100 mM NaCl, 50 mM HEPES pH 8.5. A flow rate of 0.5 mL/min was used and fractions of 100 µL were collected. SAXS data were collected at the European Synchrotron Radiation Facility (Grenoble, France) at the BM29 BioSAXS beamline. The scattering profiles measured at three protein concentrations: 1.1 and 2.2 and 3.5 mg/mL, calculated from the absorption at 280 nm, were processed with the Primus program from the ATSAS suite [15].

2.9. Cell growth under over-activation of the Zra system

One mL of a preculture containing *E. coli* W3110-*ΔzraP* transformed with pBad18-*zraS* was added to 50 mL of LB medium plus 20 µg/mL chloramphenicol. Cells were then grown at 37°C and 200 rpm with or without 0.1% arabinose until an $OD_{600nm} \approx 0.5$. For both conditions, cultures were split into two equal volumes; one of which was treated with 500 µM $ZnSO_4$. Growth was then followed by

measuring the OD_{600nm} for 4 hours. The growth rate (ΔOD_{600nm}/hour) was calculated over the period between zinc addition and OD_{600nm} = 2.

The activation of the Zra system was verified by immunoblotting with anti-ZraR antibodies (supplementary, Fig. S6) between the time of zinc addition and when the cell culture reached an OD_{600nm} of 2

3. Results and discussion

3.1. The soluble periplasmic domain of ZraS is correctly folded.

The sequence of the periplasmic domain of ZraS (ZraSp), encompassing residues 37 to 202, was identified by predicting the position of the two surrounding transmembrane helices (TM) with TMpred [16]. The soluble protein was purified in two steps, by Strep-Tactin followed by gel filtration chromatography. It resulted in electrophoretically pure ZraSp (Fig. 1A). However, the presence of three major peaks in the elution profile of the gel filtration suggested that ZraSp oligomerizes into different states (Fig. 1A). SEC-MALLS on the pooled fractions (Fig. 1B) indicates that the highest peak contains a homogenous species of about 22.9 KDa, consistent with the expected molecular weight of monomeric strep-tagged ZraSp (20.15 kDa). The other peak is less homogeneous and gives an average mass of 62 kDa that may correspond to trimers. Based on these data, only fractions from the second peak, eluted after gel filtration, were kept for further experiments. These results also show that, like most histidine kinase sensors, the purified periplasmic domain is monomeric even though the full size membrane- anchored protein is expected to be homodimeric [2].
To test the ability of the protein to dimerize at higher concentration, cross-linking experiments were performed with formaldehyde (spacer arm ≈ 2 Å [17]). After concentration by ultrafiltration, ZraSp was incubated in the presence of formaldehyde and analyzed by SDS-PAGE (Fig. 1C). The small band at a position corresponding to twice the monomer's molecular weight (40.3 kDa), indicates that dimers were covalently bonded. Thus, at high concentration, the ZraS periplasmic domain can form dimers. However, this form is unstable and fully dissociates at low concentration.

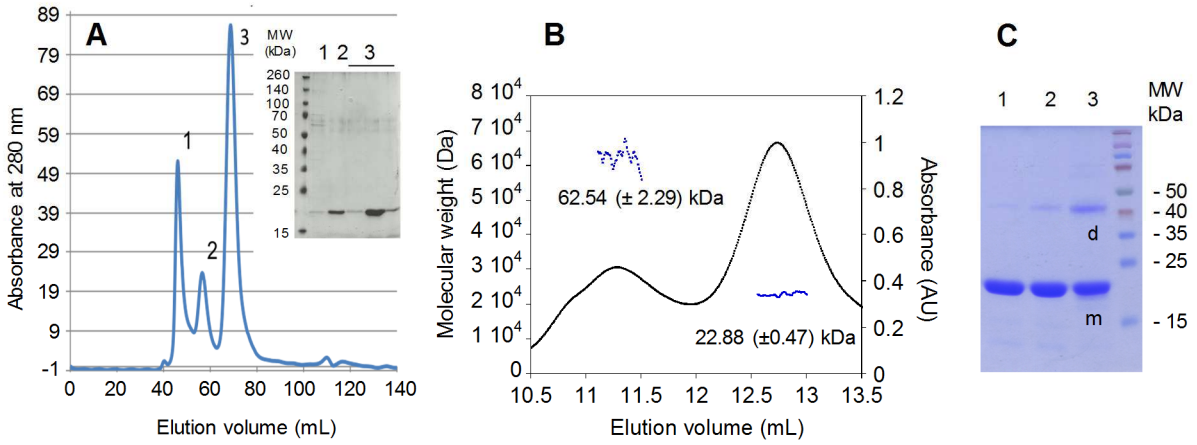

Figure 1. Characterization of Purified ZraSp. (A) Elution profile after gel filtration on HiLoad 16/60 Superdex 75 column (Amersham Biosciences). Inset: analysis of the proteins from peaks 1 to 3 by SDS-PAGE. (**B**) Analysis of pooled fractions 2 and 3 by SEC-MALLS; the elution profile and the calculated molecular weights are shown in black and blue, respectively. The average molecular weights and standard deviations are indicated in kDa. **(C)** SDS–PAGE (15% acrylamide) after cross-linking of 80 µM ZraSp with 100 (well 2) or 500 (well 3) molar ratio equivalents of formaldehyde; well 1 contains untreated protein. The molecular mass calculated from the amino acid sequence of strep-tagged ZraSp is 20,148 Da; m: position of ZraSp monomers; d: position of ZraSp dimers.

The secondary structure of purified ZraSp was analyzed by circular dichroism (CD) spectroscopy. The CD spectrum (Fig. 2A) displays two negative minima at 208 nm and 222 nm, which are typical of partially helical proteins. Calculation of the percentages of secondary structure elements by spectra deconvolution with Dichroweb [12,13] reveals 33% α-helices, 15 % β-strands and 32% unfolded regions , which is close to the secondary structure predictions by Jpred [18] from the amino acid sequence: 31.3% and 19.7% α-helices and β-strands, respectively (Fig. 2B, supplementary Table 1). These data indicate that the secondary, and almost certainly the tertiary structure, are representative of the domain in the full-length protein even when ZraSp is at low concentration and monomeric. Analysis of the secondary structure predictions also shows that the ZraS periplasmic domain has a PhoQ-DcuS-CitA (PDC) fold with a long N-terminal α-helix and a central β-sheet core flanked by short helices on both sides [19].

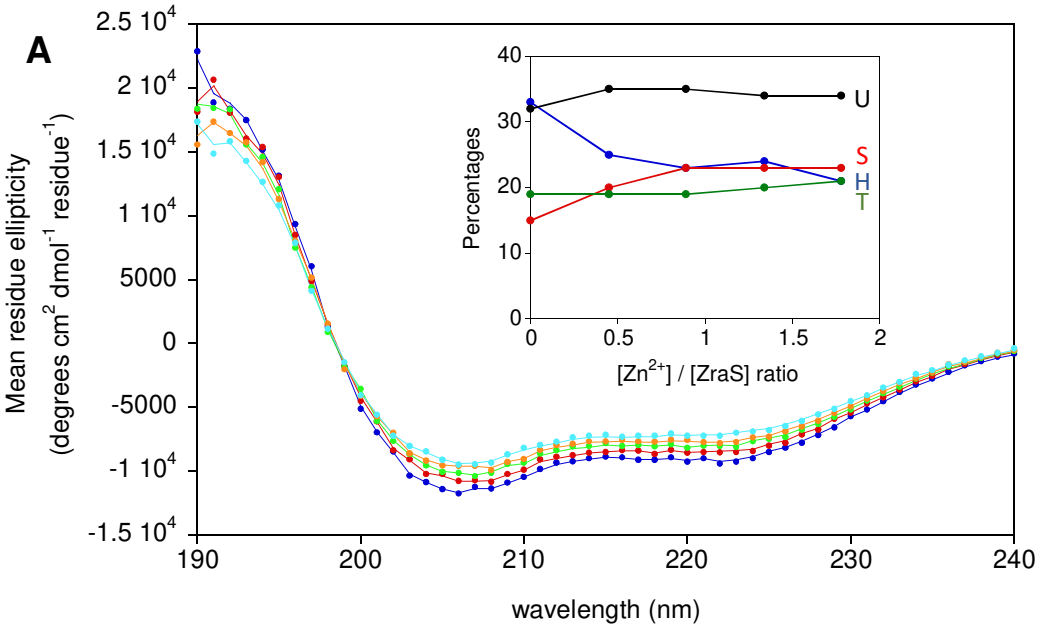

B

```
MDYGRASEADRQALLEKGNVLIRALESGSRVGMGMRMHHVQQQALLEEMAGQPGVL
---HHHHHHHHHHHHHHHHHHHHHHHHHHHHHH------HHHHHHHHHHH----BB
WFAVTDAQGIIILHSDPDKVGRALYSPDEMQKLKPEENSRWRLLGKTETTPALEVY
BBBBB----BBBBB------------------------BBBBBB------BBBBB
RLFQPMSAPWRHGMHNMPRCNGKAVPQVDAQQAIFIAVDASDLVATQSGEKRNT
BBBBB--------------------------BBBBB--HHHHHHHHHHH----
```

Figure 2. Secondary structure of apo and Zn^{2+}-bound ZraSp. (A) CD spectra of 3.54 µM ZraSp in 20 mM potassium-phosphate buffer (pH 7.5) before (blue) and after successive addition of $ZnSO_4$ to 0.45 (red), 0.89 (green), 1.34 (orange), 1.78 (cyan) molar ratio equivalents. Inset: secondary structural changes as a function of zinc concentration, values are listed in supplementary Table S1. **(B)** ZraSp sequence and secondary structure prediction by Jpred4 [18]. H: helices, S: β-strands, T: turns, U: unordered.

3.2. ZraS contains one high affinity zinc binding site

ZraS was shown to be activated by zinc, *in vivo*, which led to the so far undemonstrated conclusion that this metal ion is able to bind to the periplasmic domain of ZraS. Quantification of Zn^{2+} binding sites was carried out by inductively coupled plasma atomic emission spectroscopy (ICP-AES). Purified ZraSp was treated with a 4-fold excess of $ZnSO_4$ in the presence of either EGTA or EDTA. In the absence of chelator the protein precipitated, probably due to unspecific binding of the metal ions when present in excess. The ZraS sequence is rich in zinc-binding residues such as histidines (5), aspartates (9) and glutamates (11), most of which are located on unstructured, and therefore flexible, regions (Fig. 2). These residues can generate non-specific intermolecular binding sites, particularly at the high protein concentrations used in the test. Such adventitious binding of metal ions to protein surfaces is commonly observed [20]. Free and either EGTA- or EDTA-bound Zn^{2+} was removed by dialysis before analysis. Quantification did not reveal significant amounts of Zn^{2+} in the control sample that was only dialyzed (Zn^{2+}-ZraSp molar ratio of 0.01) nor in the sample pre-treated with EDTA (Zn^{2+}/ZraSp ratio of 0.08). By contrast, zinc ions were detected in the EGTA-treated sample with a molar ratio of 1.09. The detection of zinc in ZraSp after EGTA treatment shows that the protein has a the high affinity for this ion, since the K_d value of the EGTA-Zn^{2+} complex is 4.1×10^{-10} M, [20]. A similar result was obtained using the 4-(2-pyridylazo)resorcinol (PAR) assays [21] (supplementary Fig. S1). In this latter experiment a 7-fold excess of $ZnSO_4$ was added in the presence of EGTA, before dialysis. The analysis of the absorbance evolution at 500 nm upon gradual addition of Zn^{2+}-loaded ZraP revealed a final 0.8 Zn^{2+}-to-protein molar ratio, indicating the presence of one high-affinity Zn^{2+} binding site per monomer. This result is consistent with the presence of one ligand binding pocket in structurally characterized PDC histidine kinase sensor domains [22]. The ZraSp sequence was then analyzed using the sequence homology-based predictor PredZinc software [23], which failed to predict zinc-binding residues. As mentioned above, ZraS contains a large number of residues potentially involved in zinc binding sites; and these residues are spread throughout the sequence, making prediction very difficult.

In order to screen for other ZraS metal ligands, and similarly to what was previously published for ZraP [8,24], an *E. coli* cell lysate after ZraSp over-expression was loaded onto Zn^{2+}-, Cu^{2+}- and Cd^{2+}-NTA columns. Two different buffer solutions, respectively containing 100 and 500 mM imidazole, were successively run through the columns and the fractions were analyzed by SDS-PAGE (supplementary Fig. S2). ZraSp was retained by the Zn^{2+}-NTA and Cu^{2+}-NTA resins and was eluted by the addition of 500 mM imidazole. The protein did not bind to the Cd^{2+}-NTA resin (data not shown). The affinity of ZraSp is probably slightly lower for Zn^{2+} than for Cu^{2+}. This is suggested by the presence of ZraS in the fraction from the Zn^{2+} column washed with the 100 mM imidazole buffered solution, which was not detected with the Cu^{2+} column under the same conditions. These results are identical to those found with zrapP. However, four of the coordination sites of the metal ions are occupied by the NTA chelator. Consequently, these results are only indicative, as they do not reflect the binding of free metal ions.

3.3. Zinc binding to ZraS periplasmic domain induces conformational changes

The thermal stability of ZraSp was measured in both the presence and absence of Zn^{2+} by differential scanning fluorimetry (DSF). Modification of the tryptophan fluorescence emission intensity was followed at 350 and 330 nm. The resulting curves (Fig. 3) display two transition phases; however, the second phases were not analyzed because they very likely correspond to protein precipitation. The first phases fitted well to the two-state model equation of thermal denaturation (see materials and methods) with R-values above 0.998 and allowed melting temperature (T_m) calculations (supplementary Table S2). The isolated periplamic ZraS domain is rather unstable, with a T_m of only 33 °C. Analysis of five independent experiments show that the gradual zinc addition slightly reduces the T_m , up to a 1:1 Zinc/ZraSp ratio (Fig. 3). However, interpretable results could not be obtained for ratios > 1.25, due to protein precipitation. It suggests that zinc addition may induces very small-amplitude ZraSp conformational changes, as shown by the decrease of about than 0.5°C of *Tm*. It should be noted that the decrease of the starting fluorescence as a function of Zn^{2+} concentration reflects a quenching phenomenon (data not shown) as previously described for other zinc-bound proteins [25]. This reflects a close proximity between bound Zn^{2+} and at least one tryptophan residue.

The ability of zinc to induce structural modifications was further investigated by CD. Successive addition of zinc ions resulted in slight modifications of the spectra and their deconvolution confirmed an evolution of the secondary structure elements (Fig. 2A, supplementary Table S2) up to a 1:1 [Zn^{2+}]/[ZraSp] molar ratio, with a 10 % reduction of α-helices and a 7 % increase of β-sheets. In parallel, unordered regions and β-turns remained almost constant for all tested Zn^{2+} concentrations.
Both DSF and CD results are consistent with a slight change in ZraSp conformation upon zinc binding. The CD data show the modification of an α-helix upon zinc binding, which may reflect a piston-sliding motion mechanism, as proposed for several HK sensors such as NarX and TorS or NarQ [26–28]. A structure of NarQ encompassing the sensor domain, the transmembrane helices and the HAMP intracellular signal relay, has been recently published in both apo and NO_3-bound forms [28]. Comparison of the structures reveals a piston-like mechanism, upon ligand binding, with a relative displacement of the TMs of 2.5 Å. Similarly, a displacement of about 1 Å between the N- and C-terminal helices of the periplasmic domain, was detected between apo and nitrate-bound NarX [26]. This observation suggests that a very small conformational change in the sensor domain can be transmitted to the DHp (dimerization Histidine phosphotransfer) and CA catalytic domains, via the intracellular signal relay domain (HAMP, PAS or GAF domain) [2]. However, and remarkably, in ZraS, the 22 amino acids-long sequence between the second transmembrane helix (TM2) and the conserved DHp domain does not have enough residues (Supplementary Fig. S3) to correspond to any type of signal relay domain. This, in turn, implies a direct transmission of the signal to the DHp domain, without motion amplification.

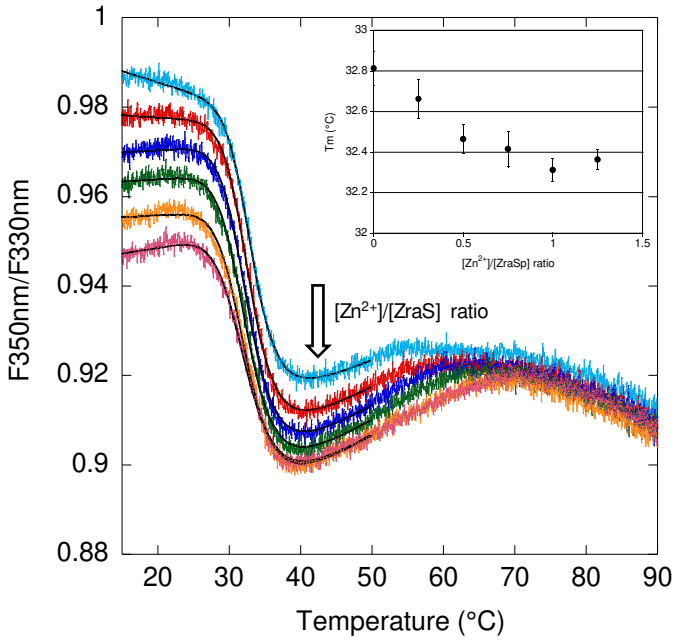

Figure 3. Thermal stability of apo and Zn^{2+}-bound ZraSp. Differential scanning fluorescence was measured with 50 µM ZraSp and increasing $ZnSO_4$ concentrations. To calculate the melting temperature (T_m), data were fitted to the two-state model shown in the materials and methods section (black lines), T_m values and statistics are presented in the supplementary (Table S2). Inset: evolution of T_m as a function of added zinc, mean values of 5 independent experiments; error bars: standard error of the mean (SEM).

3.4. ZraP only cysteine is reduced in vivo

ZraP has been described, *in vitro*, as a tetramer of disulfide-bonded dimers [8]. However, *in vivo*, mutation of the only cysteine Cys104 into an alanine did not impair the repressor activity of ZraP, questioning the role of this conserved residue and its redox state in the periplasm. In order to further

investigate this question, the protocol from Denoncin *et al*. [29] was adapted to ZraP. These authors have shown the presence of reduced cysteines in DsbA through chemical modification with the thiol reactive AMS molecule, immediately after cell lysis, and detection of a gel shift on SDS-PAGE. Chemical modification was not necessary with ZraP, since its reduced form will migrate as monomers (12.5 kDa) and its oxidized form as dimers (25 kDa) due to intermolecular disulfide bridges. Cells were rapidly harvested and lysed with reductant-free buffer with 0.1% SDS added to denature the proteins.

In a first experiment, the *E. coli* W3110 *ΔzraR* strain was transformed by a pBad plasmid carrying *zraP*. This strain was chosen because it does not produce endogenous ZraP. Cell lysates were analyzed by western blot using a ZraP-immunized rabbit serum. The presence of multiple bands, in the absence of ZraP expression (no addition of arabinose, Fig 4A, third well), reveals that the polyclonal antibodies are poorly specific and bind several *E. coli*-contained proteins. Characterization of the bands relevant to ZraP was made by comparing the different conditions to the ZraP-free cell lysate control. An intense band below 15 kDa is visible when ZraP expression was induced with arabinose, but not in the control (Fig.4 A, well 4 and 5, surrounded band). The position of this band is consistent with a mass of 12.5 kDa, which corresponds to processed monomeric periplasmic ZraP, without its signal peptide. The presence of disulfide-bonded dimers is more difficult to establish because of the unspecific bands in the 25 kDa region that could possibly mask a weak ZraP band.

Addition of zinc ions to the cells during arabinose-induced ZraP expression did not result in a change of the 12.5 kDa band intensity (Fig 4A, well 5). This suggests that zinc does not influence the formation of disulfide bridges between ZraP subunits in the periplasm.

In a second series of experiments, the expression of endogenous ZraP was induced in wild type W3110 *E. coli* strain. A single band appeared when cells were grown in the presence of Zn^{2+}, which migrates as ZraP monomers, indicating that physiologically, the cysteine residue of ZraP is reduced. The position of monomeric ZraP in the western blot is slightly higher when it comes from a cell lysate than when it is purified. This difference, detected in recombinant and endogenous ZraP-containing cell lysates, may be due to the presence of other proteins that affect ZraP migration. Comparison of the band intensities of purified ZraP obtained by SDS-PAGE and on the western blot indicates that polyclonal anti-ZraP antibodies bind more efficiently to monomeric than to dimeric ZraP (supplementary Fig. S4). We can conclude that even if our results do not allow quantification of the relative amounts of monomers and disulfide-bonded dimers, they show that the cysteine residue of ZraP is at least partially reduced in the periplasm, i.e. it does not form a sulfide bridge with the cysteine residue from another Zrap monomer. This observation suggests that while formation of disulfide bonds occurs spontaneously *in vitro* it may not be not effectively produced in the periplasm by the Dsb redox machineries [30]. *In vivo* transcription analysis revealed that the C104A mutant behaves like the wild type protein, confirming that disulfide bridges are not essential for the function of ZraP as a repressor of ZraS activation [8]. This variant was shown to form dimers at low concentration (see below).

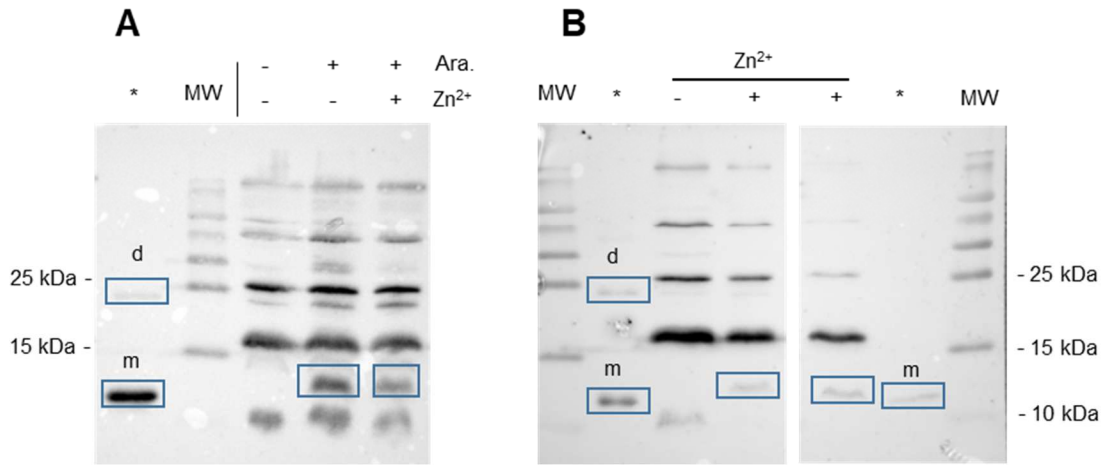

Figure 4. Redox state of C104 in the periplasm of *E.coli*. Western blot analysis of cell lysate: **(A)** *E.coli* W3110-*ΔzraR* transformed with pBad-*zraP*, the expression of recombinant ZraP was induced with 0.1% arabinose in either the presence or the absence of 500 µM $ZnSO_4$. **(B)** Expression of endogenous ZraP in *E. coli* W3110 was induced by addition of 500 µM $ZnSO_4$. The star indicates the position of purified ZraP. m: ZraP monomers, d: ZraP dimers, Ara: arabinose. 15% SDS-PAGE was run without a reducing agent and the immunoblot was revealed with anti-ZraP polyclonal antibodies.

3.5. In solution and at high concentration ZraP is a globular octamer

The structure of ZraP from *S. enterica* was deposited in the protein database in 2010, with the PDB code 3LAY. This structure includes some caveats; it does not contains zinc ions even though the protein was crystallized in the presence of 0.2 mM zinc acetate and it forms a decamer instead of the octamer later characterized in solution [8]. These discrepancies are probably due to the absence of the first 18 and the last 28 amino acid residues in the structure, which were shown to be involved in zinc bind and oligomerization, respectively [8]. However, because the folding of the dimer structure is highly similar to that of other proteins such as CpxP or Spy [5,31,32], the structure of the monomers and their organization as dimers are probably correct. SAXS experiments were carried out in order to get more information about the ZraP overall structure. Scattering curves were measured at three protein concentrations and data were processed with the Primus program [15] from the ATSAS (version 3.0.2) suite (Fig. 5A, supplementary Fig. S5 and Table S3). I_0 values are similar for all concentrations indicating that the shape and the aggregation state of the protein do not change as a function of the concentration. Additional analyses were performed with the highest concentration, 3.5 mg/mL, which gives the lowest signal-to-noise ratio at high q values. The linearity of the Guinier plots confirms that the sample is monodisperse and the Kratky plots, with bell-shaped curves and a well-defined maximum, indicate that the protein is properly folded (supplementary Fig. S5). The pair distance distribution function represents a curve with a Dmax of 7.46 nm and a well-defined maximum around Dmax/2, which shows that ZraP is a globular protein in solution (Fig. 5A). Calculation of the molecular weight gives a value of 83.08 kDa, which is lower than the expected value of 100 kDa, calculated from the amino acid sequence. The error of molecular weight determination by SAXS generally does not exceed 10 %, however, Mylonas *et al*. reported a few cases with higher discrepancies [33]. The scattering curve, generated by Crysol with the coordinates of ZraP from *S. enterica* (PDB code 3LAY) (Fig. 5A), highlights the differences between the X-ray structure and the structure in solution. The initial values (I_0) confirms that in the crystal ZraP has a higher molecular weight and the differences in the curves that the envelopes shapes are significantly dissimilar, which is obvious when inspecting the model generated with Damaver (Fig. 5B). The model does not correspond to a hollow sphere nor to a ring. The difference between the structure in solution and in the crystal may arise from the difference of the oligomerization state; in the decamer the diameter is larger than in the octamer, that would leave an empty space in the center. The N-and C-terminal extremities are most probably localized in the center of the protein but are too flexible to be detected by X-ray crystallography while they are visible with SAXS.

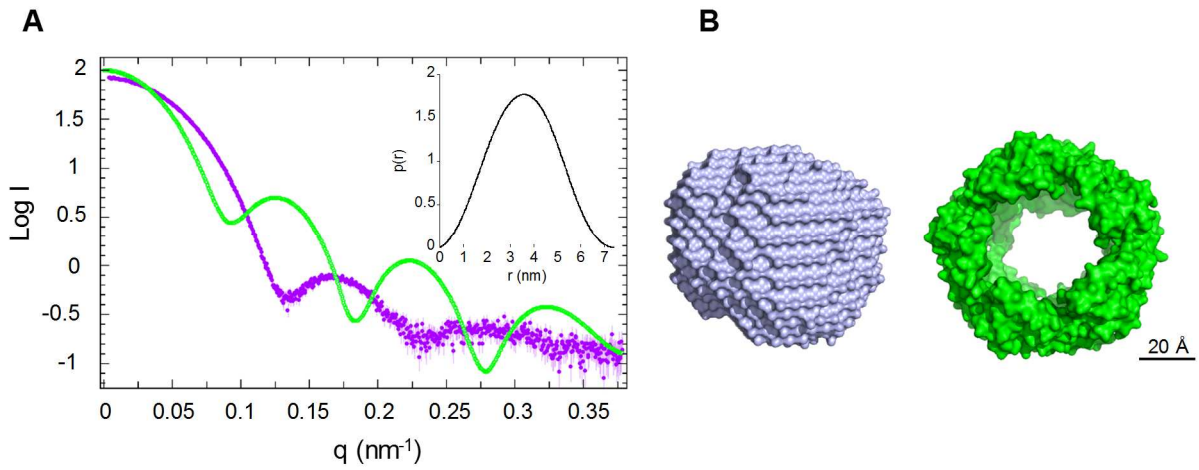

Figure 5. SAXS analysis of ZraP. **(A)** Scattering curve (violet) and pair distance distribution function (inset) of ZraP in solution; simulated scattering curve of ZraP generated with CRYSOL from the PDB 3LAY coordinates (green). **(B)** *Ab initio* model generated by the Damaver program (violet) and surface representation of ZraP X-ray structure (green). Both images are displayed at the same scale.

Mutation of Cys104 to alanine as well as the deletion of the last 7 C-terminal amino acids were shown to destabilize the octameric quaternary structure [8]. Data on analytical ultracentrifugation revealed that while only octamers were detected at 0.5 mg/mL (40 µM) with wild type ZraP, lower molecular weight species corresponding to dimers, tetramers and hexamers were detected with C104A-ZraP, at the same concentration. Increasing the concentration of the variant resulted in an increase of the hexamer content and upon zinc addition only octameric structures were formed. This demonstrates that, in the absence of disulfide bridges, and at low concentration, ZraP forms complexes smaller than octamers, the minimum size being dimers. It also shows that Zn^{2+}binding at the subunits' interface promotes the oligomerization up to the octamer species. Notably, this stabilized the C-terminal residues, without forming disulfide bridges. SAXS experiments were performed without zinc but at high concentration, which promotes oligomerization.

3.6. Over-activation of the Zra system reduces cell division rate

In order to test the effect of overactivating the Zra system, cells lacking *zraP* (*E. coli* W3110 *ΔzraP*) and over-expressing ZraS, from a pBad-*zraS* plasmid were grown. A 500 µM $ZnSO_4$ concentration was used for optimal induction without lethal effect [8,11,24]. Figure 6A shows very similar curves for cells grown in the presence or in the absence of arabinose, indicating that cell division is not affected by ZraS over-expression. Addition of zinc ions causes a reduction of the growth rate, which is significantly more pronounced when the metal ion was added to cells over-expressing ZraS than to cells grown in the absence of arabinose (Fig. 6B). This negative influence of ZraS concentration on cell division upon Zn^{2+} addition confirms that a too- high activation of the Zra system is deleterious, and shows the need of fine regulation to allow a specific response while protecting the cell. The importance of such fine-tuning was previously found with the Cpx system for which the use of a constitutively active *CpxA HK sensor* mutant resulted in cell division, growth and shape abnormalities [34].

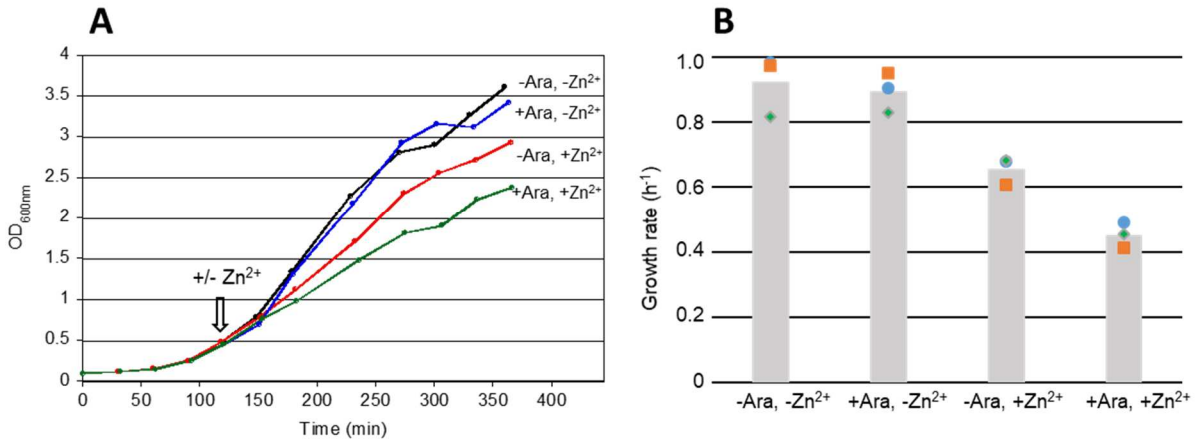

Figure 6. *E. coli* growth under condition of Zra system over-activation. (A) *E. coli* W3110-*ΔzraP* transformed with pBad18-*zraS* and grown at 37°C in either the absence (-ara) or presence (+ara) of 0.1% arabinose with (+Zn^{2+}) or without (-Zn^{2+}) addition of 500 µM $ZnSO_4$ at OD_{600nm} ≈ 0.5 (red, green), (see arrow). **(B)** The growth rates (ΔOD_{600nm}/hour) were calculated in three independent experiments (orange squares, blue circles and green diamonds), the mean values are represented by the gray histogram. The activation level of the Zra system was verified by immunoblotting on cell lysates with ZraR polyclonal antibodies (supplementary Fig. S6).

3.7. General mechanism

Because ZraP contains 72% of the zinc present in soluble proteins of *E. coli* grown in the presence of 0.2 mM Zn^{2+} [35], this protein was initially proposed to function as either a Zn^{2+} scavenger or a zinc storage protein. However, none of these functions have been confirmed; moreover, it was shown that the Zra system is not involved in protecting the cell against zinc toxicity nor in zinc homeostasis.Another possibility is that ZraP prevents ZraS activation by making zinc unavailable. The H1A variant that is deficient for zinc binding is inactive *in vivo* [8], confirming the need of zinc for repression. However, the ΔC-terminus variant, which binds the same amount of zinc as the wild type, is not active as a repressor *in vivo* [8], suggesting that zinc binding to ZraP is not sufficient and that a direct interaction between ZraP and ZraS is essential for inhibition. Taken together, previously published results, along with those described in this report, allow us to propose a mechanism for the interplay between ZraP, ZraS and zinc ions (Fig. 7). It is based (i) on the fact that zinc can bind both ZraP and ZraS, (ii) on the finding that the ZraP cysteines can be reduced in the periplasm, (iii) on the published result showing that ZraP C104A variant could be dimeric in the absence of the metal ion at low concentration and form octamers upon zinc addition [8]. In that mechanism, Zn^{2+} binding to the periplasmic ZraS domains induces a conformational change that is transmitted to the histidine kinase domain. This conformational change leads to ZraR activation, which eventually regulates its regulon [11] and, notably, also the *zra* genes. Simultaneously, zinc ions can bind to ZraP, at the interface between subunits [8] causing the oligomerization of the dimers into octamers. In this quaternary structure, ZraP inhibits ZraS by direct interaction, either by interfering with the metal binding sites or by preventing conformational changes. Overall, a fine-tuning of the TCS results in the combined presence of active and inhibited ZraS dimers.

This proposed mechanism differs in some respects from the one of the well-described Cpx sytem [3]. CpxP represses CpxA in the resting state under non-inducing conditions, whereas the repression activity of ZraP occurs at the same time as the activating process. Another significant difference is that despite the high structural homology between CpxP and ZraP dimers, the interaction of ZraP with ZraS involves the convex face of the dimers, which constitutes the exposed face of the octamer, while dimeric CpxP interacts with CpxA via its concave surface by polar interactions [5].

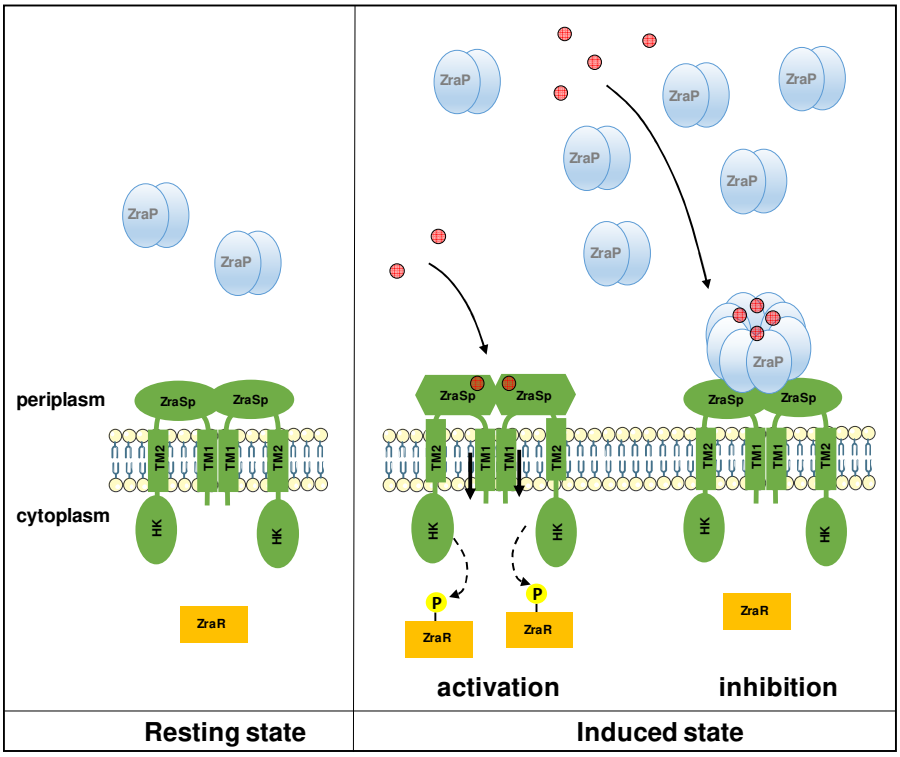

Figure 7. Schematic overview of the Zra pathway under inducing conditions. In the absence of zinc ions (resting state), the expression of the Zra system is at a basal level, ZraP (light blue ellipses) is dimeric and ZraS (green) is not active, maintaining ZraR (orange) unphosphorylated. In the presence of zinc ions (induced state), Zn^{2+} can bind to the ZraS periplasmic domains (ZraSp) leading to a conformational change that is transmitted to the histidine kinase domain (HK), possibly by a piston-like movement of the transmembrane helices (TM, solid straight arrows). This activation enables the transfer of a phosphoryl group from the HK domain to the response regulator ZraR (dashed arrows). Simultaneously to ZraS activation, Zn^{2+}can bind to ZraP, causing the oligomerization of the dimers into octamers, which bind to the ZraSp sensor domains preventing ZraS activation. Ultimately, in the induced state, active and inactive forms of ZraS coexist, resulting in a fine-tuning of the system.

4. Conclusion

Biochemical and biophysical experiments have allowed us to provide new information on the Zra system and notably on the role of zinc ions. We confirm that ZraS directly responds to Zn^{2+}, since its binding to the high affinity site induces conformational changes of the periplasmic domain. This is consistent with its protein sensor function in the TCS. We also highlight the importance of the repressor function of ZraP in protecting the cell against a too high activation of the Zra system. Finally, we show that the single ZraP cysteine residue remains reduced *in vivo*, indicating that this protein does not form intermolecular disulfide bonds in the periplasm. ZraP is initially dimeric and only oligomerizes to its repressing octameric form when the periplamic zinc concentration augments beyond a certain threshold.

Availability of data and material

Requests for data and material can be made by contacting the corresponding author.

Funding

Raleb Taher was supported by a grant from Université Grenoble Alpes (IRS—2015).

Authors' contributions

Eve de Rosny: Conceptualization, Investigation, Writing - Original Draft, Visualization, Project administration, Funding acquisition. Raleb Taher: Conceptualization, Investigation, Writing - Review & Editing.

Acknowledgments

We thank Franck Gabel for helping in the analysis of SAXS data, Julien Pérard and the Laboratory of Chemistry and Biology of Metals, for performing the ICP-AES experiments and providing access to the CD spectrophotometer. We also thank Juan C. Fontecilla-Camps and Patricia Amara for proofreading and constructive comments, as well as Océane Mangel for her help with the project during her internship. This work used the platforms of the Grenoble Instruct-ERIC center (ISBG; UMS 3518 CNRS-CEA-UGA-EMBL) within the Grenoble Partnership for Structural Biology (PSB), supported by FRISBI (ANR-10-INBS-05-02) and GRAL, financed within the University Grenoble Alpes graduate school (Ecoles Universitaires de Recherche) CBH-EUR-GS (ANR-17-EURE-0003). IBS acknowledges integration into the Interdisciplinary Research Institute of Grenoble (IRIG, CEA).

References

[1] P. Ortet, D.E. Whitworth, C. Santaella, W. Achouak, M. Barakat, P2CS: updates of the prokaryotic two-component systems database, Nucleic Acids Res. 43 (2015) D536-541. https://doi.org/10.1093/nar/gku968.

[2] F. Jacob-Dubuisson, A. Mechaly, J.-M. Betton, R. Antoine, Structural insights into the signalling mechanisms of two-component systems, Nat. Rev. Microbiol. 16 (2018) 585–593. https://doi.org/10.1038/s41579-018-0055-7.

[3] S.L. Vogt, T.L. Raivio, Just scratching the surface: an expanding view of the Cpx envelope stress response, FEMS Microbiol Lett. 326 (2012) 2–11. https://doi.org/10.1111/j.1574-6968.2011.02406.x.

[4] T.L. Raivio, M.W. Laird, J.C. Joly, T.J. Silhavy, Tethering of CpxP to the inner membrane prevents spheroplast induction of the cpx envelope stress response, Mol. Microbiol. 37 (2000) 1186–1197. https://doi.org/10.1046/j.1365-2958.2000.02074.x.

[5] X. Zhou, R. Keller, R. Volkmer, N. Krauss, P. Scheerer, S. Hunke, Structural basis for two-component system inhibition and pilus sensing by the auxiliary CpxP protein, J. Biol. Chem. 286 (2011) 9805–9814. https://doi.org/10.1074/jbc.M110.194092.

[6] K. Tschauner, P. Hörnschemeyer, V.S. Müller, S. Hunke, Dynamic interaction between the CpxA sensor kinase and the periplasmic accessory protein CpxP mediates signal recognition in *E. coli*, PLoS ONE. 9 (2014) e107383. https://doi.org/10.1371/journal.pone.0107383.

[7] C. Appia-Ayme, A. Hall, E. Patrick, S. Rajadurai, T.A. Clarke, G. Rowley, ZraP is a periplasmic molecular chaperone and a repressor of the zinc-responsive two-component regulator ZraSR, Biochem. J. 442 (2012) 85–93. https://doi.org/10.1042/BJ20111639.

[8] I. Petit-Härtlein, K. Rome, E. de Rosny, F. Molton, C. Duboc, E. Gueguen, A. Rodrigue, J. Covès, Biophysical and physiological characterization of ZraP from *Escherichia coli*, the periplasmic accessory protein of the atypical ZraSR two-component system, Biochem. J. 472 (2015) 205–216. https://doi.org/10.1042/BJ20150827.

[9] L. van der Weel, K.S. As, W.J.C. Dekker, L. van den Eijnden, W. van Helmond, C. Schiphorst, W.R. Hagen, P.-L. Hagedoorn, ZraP, the most prominent zinc protein under zinc stress conditions has no direct role in in-vivo zinc tolerance in E*scherichia coli*, J. Inorg. Biochem. 192 (2019) 98–106. https://doi.org/10.1016/j.jinorgbio.2018.12.013.

[10] S. Leonhartsberger, A. Huber, F. Lottspeich, A. Böck, The hydH/G Genes from *Escherichia coli* code for a zinc and lead responsive two-component regulatory system, J. Mol. Biol. 307 (2001) 93–105. https://doi.org/10.1006/jmbi.2000.4451.

[11] K. Rome, C. Borde, R. Taher, J. Cayron, C. Lesterlin, E. Gueguen, E. De Rosny, A. Rodrigue, The Two-Component System ZraPSR Is a Novel ESR that Contributes to Intrinsic Antibiotic Tolerance in *Escherichia coli*, J. Mol. Biol. 430 (2018) 4971–4985. https://doi.org/10.1016/j.jmb.2018.10.021.
[12] L. Whitmore, B.A. Wallace, DICHROWEB, an online server for protein secondary structure analyses from circular dichroism spectroscopic data, Nucleic Acids Res. 32 (2004) W668-673. https://doi.org/10.1093/nar/gkh371.
[13] N. Sreerama, R.W. Woody, Estimation of protein secondary structure from circular dichroism spectra: comparison of CONTIN, SELCON, and CDSSTR methods with an expanded reference set, Anal. Biochem. 287 (2000) 252–260. https://doi.org/10.1006/abio.2000.4880.
[14] V. Consalvi, R. Chiaraluce, L. Giangiacomo, R. Scandurra, P. Christova, A. Karshikoff, S. Knapp, R. Ladenstein, Thermal unfolding and conformational stability of the recombinant domain II of glutamate dehydrogenase from the hyperthermophile Thermotoga maritima, Protein Eng. 13 (2000) 501–507.
[15] P.V. Konarev, V.V. Volkov, A.V. Sokolova, M.H.J. Koch, D.I. Svergun, PRIMUS: a Windows PC-based system for small-angle scattering data analysis, J Appl Cryst. 36 (2003) 1277–1282. https://doi.org/10.1107/S0021889803012779.
[16] J. Hofmann, Landesregierungen als Akteure in der Technologieförderung, in: J. Hofmann (Ed.), Implizite Theorien in der Politik: Interpretationsprobleme regionaler Technologiepolitik, VS Verlag für Sozialwissenschaften, Wiesbaden, 1993: pp. 166–207. https://doi.org/10.1007/978-3-322-94245-6_7.
[17] O.W. Nadeau, G.M. Carlson, Protein Interactions Captured by Chemical Cross-linking: One-Step Cross-linking with Formaldehyde, Cold Spring Harb Protoc. 2007 (2007) pdb.prot4634. https://doi.org/10.1101/pdb.prot4634.
[18] JPred4: A Protein Secondary Structure Prediction Server, (n.d.). https://pubmed-ncbi-nlm-nih-gov.insb.bib.cnrs.fr/25883141/ (accessed July 7, 2020).
[19] J. Cheung, C.A. Bingman, M. Reyngold, W.A. Hendrickson, C.D. Waldburger, Crystal structure of a functional dimer of the PhoQ sensor domain, J. Biol. Chem. 283 (2008) 13762–13770. https://doi.org/10.1074/jbc.M710592200.
[20] Z. Xiao, A.G. Wedd, The challenges of determining metal-protein affinities, Nat Prod Rep. 27 (2010) 768–789. https://doi.org/10.1039/b906690j.
[21] K.A. McCall, C.A. Fierke, Colorimetric and fluorimetric assays to quantitate micromolar concentrations of transition metals, Anal. Biochem. 284 (2000) 307–315. https://doi.org/10.1006/abio.2000.4706.
[22] Z. Zhang, W.A. Hendrickson, Structural Characterization of the Predominant Family of Histidine Kinase Sensor Domains, J Mol Biol. 400 (2010) 335–353. https://doi.org/10.1016/j.jmb.2010.04.049.
[23] N. Shu, T. Zhou, S. Hovmöller, Prediction of zinc-binding sites in proteins from sequence, Bioinformatics (Oxford, England). 24 (2008) 775–782. https://doi.org/10.1093/bioinformatics/btm618.
[24] M. Noll, K. Petrukhin, S. Lutsenko, Identification of a novel transcription regulator from Proteus mirabilis, PMTR, revealed a possible role of YJAI protein in balancing zinc in *Escherichia coli*, J. Biol. Chem. 273 (1998) 21393–21401. https://doi.org/10.1074/jbc.273.33.21393.
[25] J.M. Butkus, S. O'Riley, B.S. Chohan, S. Basu, Interaction of Small Zinc Complexes with Globular Proteins and Free Tryptophan, International Journal of Spectroscopy. 2016 (2016) 1378680. https://doi.org/10.1155/2016/1378680.
[26] J. Cheung, W.A. Hendrickson, Structural analysis of ligand stimulation of the histidine kinase NarX, Structure. 17 (2009) 190–201. https://doi.org/10.1016/j.str.2008.12.013.

[27] J.O. Moore, W.A. Hendrickson, Structural analysis of sensor domains from the TMAO-responsive histidine kinase receptor TorS, Structure. 17 (2009) 1195–1204. https://doi.org/10.1016/j.str.2009.07.015.
[28] I. Gushchin, I. Melnikov, V. Polovinkin, A. Ishchenko, A. Yuzhakova, P. Buslaev, G. Bourenkov, S. Grudinin, E. Round, T. Balandin, V. Borshchevskiy, D. Willbold, G. Leonard, G. Büldt, A. Popov, V. Gordeliy, Mechanism of transmembrane signaling by sensor histidine kinases, Science. 356 (2017). https://doi.org/10.1126/science.aah6345.
[29] K. Denoncin, V. Nicolaes, S.-H. Cho, P. Leverrier, J.-F. Collet, Protein disulfide bond formation in the periplasm: determination of the in vivo redox state of cysteine residues, Methods Mol. Biol. 966 (2013) 325–336. https://doi.org/10.1007/978-1-62703-245-2_20.
[30] K. Denoncin, J.-F. Collet, Disulfide bond formation in the bacterial periplasm: major achievements and challenges ahead, Antioxid. Redox Signal. 19 (2013) 63–71. https://doi.org/10.1089/ars.2012.4864.
[31] G.L. Thede, D.C. Arthur, R.A. Edwards, D.R. Buelow, J.L. Wong, T.L. Raivio, J.N.M. Glover, Structure of the periplasmic stress response protein CpxP, J. Bacteriol. 193 (2011) 2149–2157. https://doi.org/10.1128/JB.01296-10.
[32] S. Quan, P. Koldewey, T. Tapley, N. Kirsch, K.M. Ruane, J. Pfizenmaier, R. Shi, S. Hofmann, L. Foit, G. Ren, U. Jakob, Z. Xu, M. Cygler, J.C.A. Bardwell, Genetic selection designed to stabilize proteins uncovers a chaperone called Spy, Nat. Struct. Mol. Biol. 18 (2011) 262–269. https://doi.org/10.1038/nsmb.2016.
[33] E. Mylonas, D.I. Svergun, Accuracy of molecular mass determination of proteins in solution by small-angle X-ray scattering, J Appl Cryst. 40 (2007) s245–s249. https://doi.org/10.1107/S002188980700252X.
[34] A. Delhaye, J.-F. Collet, G. Laloux, Fine-Tuning of the Cpx Envelope Stress Response Is Required for Cell Wall Homeostasis in *Escherichia coli*, MBio. 7 (2016) e00047-00016. https://doi.org/10.1128/mBio.00047-16.
[35] A.-M. Sevcenco, M.W.H. Pinkse, H.T. Wolterbeek, P.D.E.M. Verhaert, W.R. Hagen, P.-L. Hagedoorn, Exploring the microbial metalloproteome using MIRAGE, Metallomics. 3 (2011) 1324–1330. https://doi.org/10.1039/c1mt00154j.